Nucleic Acids Research, 2025, **53**, gkaf449
https://doi.org/10.1093/nar/gkaf449
Gene regulation, Chromatin and Epigenetics

Timed chromatin invasion during mitosis governs prototype foamy virus integration site selection and infectivity

Floriane Lagadec[1,2,†], Parmit K. Singh[3,4,†], Christina Calmels[1,2], Delphine Lapaillerie[1,2], Dirk Lindemann[5,6], Vincent Parissi[1,2], Peter Cherepanov[7], Alan N. Engelman[3,4], Paul Lesbats[1,2,*]

[1]Fundamental Microbiology and Pathogenicity Lab (MFP), UMR 5234 CNRS–University of Bordeaux, SBM Department, F-33076 Bordeaux, France
[2]Viral DNA Integration and Chromatin Dynamics Network (DyNAVir), F-33076 Bordeaux, France
[3]Department of Cancer Immunology and Virology, Dana–Farber Cancer Institute, Boston, MA 02215, United States
[4]Department of Medicine, Harvard Medical School, Boston, MA 02115, United States
[5]Institute of Medical Microbiology and Virology, University Hospital and Medical Faculty "Carl Gustav Carus", Technische Universität Dresden, 01307 Dresden, Germany
[6]Center for Regenerative Therapies Dresden (CRTD), Technische Universität Dresden, 01307 Dresden, Germany
[7]Chromatin Structure and Mobile DNA Laboratory, The Francis Crick Institute, London NW1 1AT, United Kingdom

[*]To whom correspondence should be addressed. Email: paul.lesbats@u-bordeaux.fr
[†]The first two authors should be regarded as Joint First Authors.

Abstract

Selection of a suitable chromatin environment during retroviral integration is a tightly regulated process. Most retroviruses, including spumaretroviruses, require mitosis for nuclear entry. However, whether intrinsic chromatin dynamics during mitosis modulates retroviral genome invasion is unknown. Previous work uncovered critical interactions of prototype foamy virus (PFV) Gag with nucleosomes via a highly conserved arginine anchor residue. Yet, the regulation of Gag–chromatin interaction and its functional consequences for spumaretrovirus biology remain obscure. Here, we investigated the kinetics of chromatin binding by Gag during mitosis and proviral integration in synchronized cells. We showed that alteration of Gag affinity for nucleosome binding induced untimely chromatin tethering during mitosis, decreased infectivity, and redistributed viral integration sites to markers associated with late replication timing of chromosomes. Mutant Gag proteins were, moreover, defective in their ability to displace the histone H4 tail from the nucleosome acidic patch of highly condensed chromatin. These data indicate that the chromatin landscape during Gag–nucleosome interactions is important for PFV integration site selection and that spumaretroviruses evolved high-affinity chromatin binding to overcome early mitosis chromatin condensation.

Graphical abstract

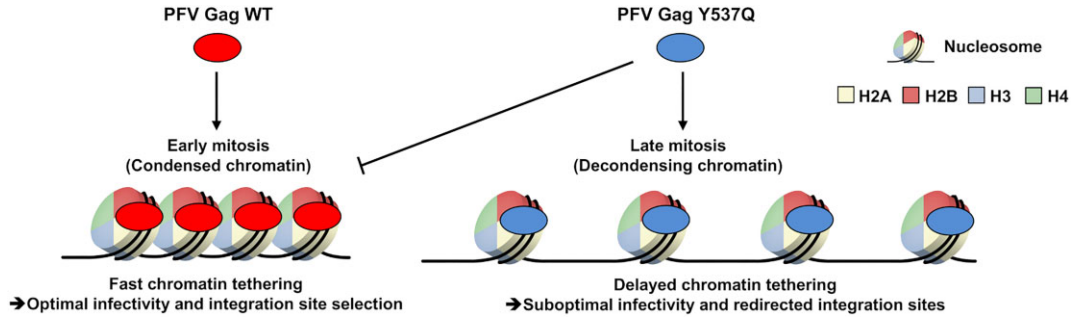

Introduction

Spumaretroviruses, also known as foamy viruses (FVs), are ancient retroviruses marked by a long co-evolutionary relationship with their hosts [1]. They are prevalent in most non-human primates (NHPs), serving as a reservoir for potential zoonotic transmissions to humans exposed to infected NHPs [2, 3]. FVs establish a persistent, lifelong infection in their human hosts. To date, no reports of severe illness or human-to-human transmission have been documented, indicating effective control of FV replication and transmission in humans [4, 5]. Prototype foamy virus (PFV) is the best studied human FV isolate, which constitutes an attractive platform for gene

Received: March 3, 2025. **Revised:** May 5, 2025. **Editorial Decision:** May 6, 2025. **Accepted:** May 15, 2025

therapy vector development [6]. Structural studies of PFV intasomes unveiled important mechanisms of retroviral integration and inhibition of integrase (IN) activity by strand transfer inhibitors [7, 8].

Integration of reverse-transcribed viral DNA into the host cell genome is a mandatory step of the retroviral replication cycle [9]. The outcome of the integrated provirus is intricately linked to the local chromatin environment dictating the expression pattern of the viral genome [10, 11]. Consequently, retroviruses have evolved genus-specific strategies to navigate within chromosomal features and select suitable chromatin landscapes [12]. Several retroviruses access cellular chromatin during mitosis when the nuclear envelope has dissipated. The impact of mitotic chromosomal condensation dynamics on the process of retroviral integration is, however, poorly documented. As opposed to the highly pathogenic lentivirus HIV-1, FVs appear to disfavor integration into gene-dense regions of the genome but rather target heterochromatin regions such as lamina-associated domains (LADs) [13, 14]. The mechanism of integration site selection has been extensively studied for HIV-1 [15–18], uncovering hierarchical interactions between the Gag capsid and IN proteins with cognate cellular factors [19–24]. In the case of FVs, precise molecular mechanisms responsible for integration site selection remain comparatively obscure and warrant further investigation to inform the applicability of FV-derived gene therapy vectors.

In contrast to HIV-1 and other orthoretroviruses, spumaretroviral Gag is minimally processed by the viral protease, thus sidestepping the production of individualized Gag processing products such as capsid and nucleocapsid [1]. Previously, we demonstrated a direct interaction of PFV Gag with the H2A–H2B acidic patch of host nucleosomes [14]. This interaction critically determined PFV integration targeting, as the Gag R540Q arginine anchor substitution massively redirected integration to centromeric regions of chromosomes. Building on these results, we have further characterized the molecular determinants regulating PFV Gag interaction with chromatin. In addition to the previously described Arg540 anchor residue, we identified a conserved tyrosine (Y537) that contacts the histone core. Substitution of Tyr with Gln (Y537Q) altered the ability of PFV Gag to bind nucleosomes *in vitro* and showed unexpected, untimely chromatin tethering during mitosis. These phenotypes were, moreover, associated with a unique pattern of integration site selection, establishing a relationship between mitotic phases, DNA replication timing, and PFV integration site selection.

Materials and methods

Nucleosome core particle

Recombinant nucleosome core particles (NCPs) (mononucleosomes) were assembled as previously described [13]. Briefly, individual human histones H2A, H2B, H3, and H4 were purchased (The Histone Source; Colorado State University) and octamers were assembled by dialysis. The Widom-601 DNA [25] was generated by restriction enzyme digestion of a concatenated construct and purified by anion exchange chromatography onto a POROS-HQ column. NCPs were assembled with a ratio 1.1:1 (1.1 octamer:1 DNA) by successive steps of salt dialysis against TEN buffer (0–2 M NaCl, 10 mM Tris, pH 7.5, 1 mM ethylenediaminetetraacetic acid, 1 mM Dithiothreitol (DTT)). NCPs were kept at −80°C in 0 mM NaCl TEN buffer.

Table 1. Sequences of peptides used for interaction experiments

Name of peptide	Sequence
Gag wild-type biotinylated	Biotin-GGYNLRPRTYQPQRYG-OH
Gag R540Q biotinylated	Biotin-GGYNLQPRTYQPQRYG-OH
Gag Y537Q biotinylated	Biotin-GGQNLRPRTYQPQRYG-OH
H4 wild-type biotinylated	Biotin-SGRGKGGKGLGKGGAKRHRKVLR-OH
H4 mutant biotinylated	Biotin-SGRGKGGKGLGKGGAKRHAAVLA-OH
H4 wild-type	H-SGRGKGGKGLGKGGAKRHRKVLR-OH
H4 mutant	H-SGRGKGGKGLGKGGAKRHAAVLA-OH

Peptides were chemically produced.

Pull-down assay

Twenty microliters of streptavidin beads (Dynabeads™ MyOne™ Streptavidin T1; Invitrogen; Thermo Fisher Scientific) were used per condition. StreptaBeads were washed twice with pull-down buffer (20 mM Tris–HCl, pH 7.5, 0.1% NP-40, 10% glycerol, 75–150 mM NaCl, 0.5 mM DTT, and 1 mM Phenylmethylsulfonyl fluoride (PMSF)) containing 75 mM of NaCl and 100 μg of bovine serum albumin (BSA), followed by one wash in the same conditions, without BSA. 1.5 μg of Gag CBS (chromatin binding site) biotinylated peptide and 3 μg of recombinant NCPs were added per condition, in a final volume of 800 μl of pull-down buffer with corresponding NaCl concentrations. The reaction mix was incubated for 2 h on a rotation wheel, at 4°C. Beads were washed three times with the corresponding NaCl concentration buffer, and bound proteins were eluted by the addition of 10 μl of SDS Sample Buffer 2.5×. Samples were separated by sodium dodecyl sulfate–polyacrylamide gel electrophoresis, and analyzed after colloidal Coomassie blue staining.

BLI analysis

Quantitative interaction experiments were performed by biolayer interferometry (BLI), using a BLItz instrument (Octet® N1; Sartorius). Two different runs were performed: the first one, into water, to coat biosensors with biotinylated peptides (Table 1) and the second, into Blitz buffer [1× phosphate buffer saline, pH 7.4, 0.02% (v/v) Tween 20, 0.1% (w/v) BSA], to fix NCPs on immobilized peptides. All steps were performed under 2200 rpm shaking speed. Streptavidin biosensors (Octet®SA Biosensors; Reference 18-0009; Sartorius) were first pre-wet for at least 10 min with water. The baseline, with only water, was measured for 60 s. Ten micromolar Gag CBS biotinylated peptides (or H4 biotinylated peptides), diluted in water, were loaded onto the biosensors, for 180 s, to reach a binding of ∼1.5 nm, followed by a dissociation step of 180 s. Following the first run, coated biosensors were equilibrated for at least 10 min in Blitz buffer. The second run started with 60 s of baseline, followed by the association step, where biosensors were dipped into serial dilutions of NCPs (10, 25, 50, or 100 nM), for 300 s. Finally, the dissociation step was performed in Blitz buffer, for 300 s. For competition experiments, the second run started with 60 s of baseline in Blitz buffer, followed by 300 s of association

step. During this step, solutions of 100 nM of NCPs were pre-incubated with or without 100 μM of H4 peptide [wild type (WT) or mutant, non-biotinylated], in Blitz buffer, for at least 30 min at room temperature. Finally, the dissociation step was performed in Blitz buffer, for 180 s. Nonspecific binding controls were performed, such as binding of 100 nM of NCPs on biosensors without biotinylated peptides loaded, as well as binding of Blitz buffer on loaded biosensors. For each time point measured, data of this second control (binding of Blitz buffer on biosensors loaded with biotinylated Gag WT peptide) were subtracted to every condition and were plotted on curves, using Prism 9 software.

Cell culture

Human fibrosarcoma cell line HT1080 (ATCC CCL-121) and proteoglycan-deficient packaging cell line 293T-25A [26] were maintained in Dulbecco's modified Eagle medium (DMEM; Fisher), supplemented with 50 μg/ml of gentamicin (Fisher Scientific) and 10% fetal calf serum (FCS) (Eurobio Scientific).

Viral vector production

PFV particles were produced using a four-component system, based on a protocol described in [26]. Plasmids pcoPG4 (PFV Gag), pcoPP (PFV Pol), pcoSE (SFVmac/SFVmcy Env), and puc2MD9 were co-transfected using a 4:2:1:28 ratio. Briefly, 293T-25A cells were transfected using calcium phosphate, in DMEM without FCS, for 5 h at 37°C. After 5 h, transfection medium was replaced by fresh DMEM containing 10% FCS, for 48 h at 37°C. Supernatants were harvested, filtered through a 0.45-μm filter, and either kept at −80°C or processed for viral particles' purification. Viral particles were pelleted by ultracentrifugation of supernatants, 2 h at 25 000 rpm, at 4°C, on a 20% sucrose cushion, in an SW-32Ti rotor. PFV particles were resuspended in 1× PBS supplemented with 5% Dimethyl sulfoxide (DMSO), and kept at −80°C.

Viral transductions

To analyze kinetics of PFV integration, 5×10^4 HT1080 cells were plated in each well of a 24-well plate. To remove residual contaminant plasmids, purified viral particles were treated with 1 μl of Denarase, 25 kU (20804–25k, c-LEcta), in a final volume of 200 μl of 1× PBS, for 1 h 30 min at 37°C. Synchronization of transductions was performed using spinoculation, as previously described [27]. Briefly, viral particles were added to cold DMEM, and 500 μl of viral solution was added to each well. The plate was kept 10 min at 4°C and centrifuged 30 min at 1200 × *g*, at 10°C. Infection medium was then replaced with pre-warmed DMEM. This time point was considered as the starting point (T0) of the transduction. For integration kinetic experiments, 2 μM dolutegravir (DTG) (GSK1349572, Selleckchem) (or DMSO as a control) was added at different time points post-transduction. Transduced cells were maintained for 6 days post-transduction, with fresh medium containing 2 μM DTG replaced every 2 days. Six days post-transduction, the percentage of GFP expressing cells was determined by flow cytometry analysis, as a readout of infectivity. To analyze the kinetics of integration, the condition that omitted DTG was set to 100% and this value was used to normalize earlier time points, for each virus independently. To compare the infectivity of the three viruses, the condition that omitted DTG in the PFV Gag WT transduction condition (∼70% of GFP-positive cells) was arbitrarily set to 100%, and compared to the values of the same condition for the two other viruses.

For viral transduction of synchronized cells, 3×10^4 HT1080 cells were platted in 24-well plates containing coverslips coated with 0.01% poly-L-lysine (P4832, Sigma). The day after, HT1080 cells were treated with 20 μM of RO-3306 (SML0569, Sigma), in DMEM, for 17 h at 37°C. After 17 h of treatment, the medium was replaced by 500 μl of supernatant containing viral particles, supplemented with 20 μM of RO-3306, for 1 h at 37°C. After 1 h (after a total of 18 h of RO-3306 treatment), cells were carefully washed twice with warm fresh DMEM, and 1 ml of medium was added per well. This time point was considered as the starting point (T0) of the cell cycle analysis. Cells were fixed at different time points after RO-3306 release, 10 min at room temperature with 4% paraformaldehyde (PFA) (EM-15710, Euromedex) diluted in 1× PBS. Coverslips were kept in 1× PBS at 4°C, until further immunofluorescence analysis.

Immunofluorescence

After fixation with 4% PFA, cells kept at 4°C were permeabilized for 5 min at room temperature (0.5% Triton X-100 diluted into 1× PBS) and washed twice with 1× PBS. Cells were incubated for 20 min at room temperature with IF Buffer (0.2% Triton X-100, 3% BSA diluted into 1× PBS). Primary antibodies were diluted in IF Buffer and incubated for 1 h at 37°C on cells. After two washes with 1× PBS, secondary antibodies diluted in IF Buffer were incubated on cells for 1 h at 37°C. Cells were then washed twice with 1× PBS and incubated with DAPI (D9542, Sigma) diluted 1:1000 in 1× PBS. Cells were then washed with successive baths of 1× PBS, H_2O, and absolute ethanol, coverslips were air dried, and a drop of mounting medium (Dako, Agilent) was added to seal coverslips on glass slides. Immunofluorescence analysis was performed by confocal microscopy, using a Leica TCS SP8 and the Leica LAS-X software, at the Bordeaux Imaging Center. The pinhole was set to 1, and z-stacks were collected at 0.5-μm intervals, with seven planes collected per stack. Images were acquired at a 16-bit resolution with a pixel size of ∼90 nm. Images were analyzed using the ImageJ software.

Image quantification

For image quantification, the Fiji software was used, and a semi-automated macro was designed to measure Gag–chromatin-bound signal. Channels were split and analyses were performed on z-projections of seven stacks. The cell outline was manually defined and a threshold was applied on the DAPI channel to define the chromatin region. Both the cell and chromatin areas were defined as regions of interest (ROIs) for further analyses. A threshold on the Gag channel was applied to select signals of interest. Finally, the area of Gag within the ROIs was measured, and a percentage of Gag occupancy within these ROIs was automatically determined. Percentages were plotted on a graph, using Prism 9 software, representing the percentage of Gag signal measured within the chromatin area. A minimum of five cells per condition were analyzed. Means were represented with their standard deviation.

Antibodies

For immunofluorescence analysis, the following antibodies were used: polyclonal rabbit antisera raised against PFV Gag recombinant [28], dilution 1:1000; mouse anti-

Lamin A/C (ab40567, Abcam), dilution 1:250; mouse anti-pericentrin (ab28144; abcam), dilution 1:500; mouse anti-tubulin (T6199, Merck), dilution 1:500; and donkey cross-adsorbed secondary antibodies coupled with Alexa Fluor 488, 594, or 647 (Life Technologies) were used at a dilution of 1:500. For western blot analysis, the same polyclonal antisera raised against Gag was used at a dilution of 1:1000 and HRP-conjugated anti-rabbit antibody (A8275, Sigma) was used at a dilution of 1:10 000.

Real-Time Quantitative PCR (qPCR)

One hour post-infection of HT1080 cells, DNA was extracted using the High Pure Viral Nucleic Acid Kit (Roche) according to the manufacturer's instructions. A quantitative qPCR was performed to determine the relative quantity of viral DNA (vDNA), using the GoTaq® qPCR Master Mix (Promega). Primers used to detect vDNA were designed as follows [29]: 203F—AGATTGTACGGGAGCTCTTCAC and 203R—CAGAAAGCATTGCAATCACC. The values obtained for DNA content of viral particle samples were expressed as percentage compared to the PFV Gag WT virus.

qPCR analysis was also performed to determine the relative quantification of vDNA integrated in HT1080 transduced cells. gDNA was extracted, using the Quick-DNA Miniprep Plus Kit (ZymoResearch). One hundred twenty nanograms of DNA was used per condition, and qPCR reactions were performed using the GoTaq® qPCR Master Mix. Primers 203F and 203R (described above) were used to detect vDNA, and GAPDH was used to normalize the gDNA quantity in each condition. The values obtained for vDNA detected per sample were expressed as percentage of the values obtained for a transduction with PFV Gag WT virus.

Analyses of integration site distributions

PFV integration sites for Y537Q mutant were generated for this study as previously described [14]. The BED files associated with PFV integration sites are available at https://dataverse.harvard.edu/dataset.xhtml?persistentId=doi:10.7910/DVN/PP9APV. The hg19 RefSeq genes specific to mitotic time points 0, 40, and 80 min are available at https://dataverse.harvard.edu/dataset.xhtml?persistentId=doi:10.7910/DVN/RFKDMH. We downloaded expression of mitotic genes from accession number GSE87476 [30], replication-initiation determinant protein (RepID) ChIP-seq data (GSM2123987) from accession number GSE80298 [31], and the hg38 coordinates of 10 SPIN states of the human genome from the published study [32]. Integration sites from the hg38 genome and SPIN coordinates were lifted to hg19 by the UCSC utilities LiftOver. Distributions of retroviral integration sites with respect to various genomic features were determined using BEDtools software suite [33]. Based on replication timing, human chromosomes were divided into three chromosomal groups: early (1, 15, 16, 17, 19, 20, 22), middle (3, 6, 7, 9, 10, 11, 12, 14), and late (2, 4, 5, 8, 13, 18, 21) replicating chromosomes.

Results

Invariant PFV Gag CBS residues that interact with human nucleosomes

The crystal structure of PFV Gag CBS (residues 535–550) bound to a nucleosome illuminated the molecular determinants for chromatin tethering [14]. The peptide adopts an extended conformation spanning across the histone side of the nucleosome disk (Fig. 1A). One major contact involves PFV Gag residue Arg540 projecting into the H2A–H2B acidic patch cluster formed by H2A Glu61, Asp90, and Glu92 residues (Fig. 1A, right panel). This arginine residue is referred to as arginine anchor motif and is a hallmark of many chromatin-binding factors [34]. Amino acid sequence alignment [35] of CBS regions from several FV species as well as endogenous FV elements revealed a strong evolutionary conservation of this arginine anchor motif (Fig. 1B), suggesting selective pressure to maintain Gag chromatin tethering. Further inspection highlighted that, in addition to Arg540, the invariant Tyr537 residue interacts with the H2A–H2B acidic patch, with its hydroxyl group making a hydrogen bond with the side chain of H2B residue Gln44. The PFV arginine anchor motif interaction with H2A–H2B acidic patch was shown to be crucial for chromatin tethering and integration site selection, redirecting insertion sites into centromeric regions of the genome [14]. Identification of another conserved acidic patch-interacting residue prompted us to investigate the role of Tyr537 in Gag–chromatin binding and PFV integration.

Peptides derived from PFV Gag CBS recapitulated the full-length protein interaction with recombinant nucleosomes [14]. To characterize the role of Tyr537 in nucleosome binding, we abolished its hydrophobic interaction mediated by the benzene ring while maintaining a similarly long side chain with a Gln substitution. We performed pull-down experiments using either WT, Tyr537Gln (Y537Q), or Arg540Gln (R540Q) substitutions in the context of biotinylated CBS peptides. As shown in Fig. 2A, WT CBS peptide efficiently pulled down nucleosomes across tested salt concentrations (75–150 mM NaCl). While the R540Q substitution reduced binding under hypotonic conditions, increasing salt to physiological concentrations (125–150 mM) virtually eliminated binding (Fig. 2A). The Y537Q substitution also affected nucleosome interaction, though largely in a salt-independent manner. To obtain quantitative data on the interactions between PFV Gag CBS peptides and nucleosomes, we performed BLI. Streptavidin biosensors were loaded with WT, R540Q, or Y537Q biotinylated CBS peptides and probed for interaction with various concentrations of recombinant NCPs at physiological salt concentration. Binding of nucleosomes to Gag CBS peptides induced a wavelength shift that was directly linked to the number of molecules bound to the surface of the biosensor. As expected, based on the results of the pull-down experiments, the strongest BLI interaction was observed with WT CBS peptides (Fig. 2B). For each nucleosome concentration, Y537Q and R540Q CBS peptides showed ∼5-fold and almost complete reduction of the interaction with nucleosomes, respectively. These data show that while PFV Gag arginine anchor motif at position 540 is a major determinant for NPC binding, the invariant Tyr537 residue contributes to high-affinity interaction.

Invariant CBS residues Tyr537 and Arg540 influence the timing of chromatin capture during mitosis

Mitosis is required during FV infection to gain access to host chromatin [36]. Upon cell division, nuclear envelope breakdown exposes chromatin to incoming FV particles for subsequent integration of the viral genome. To evaluate the precise role of conserved CBS residues in chromatin invasion

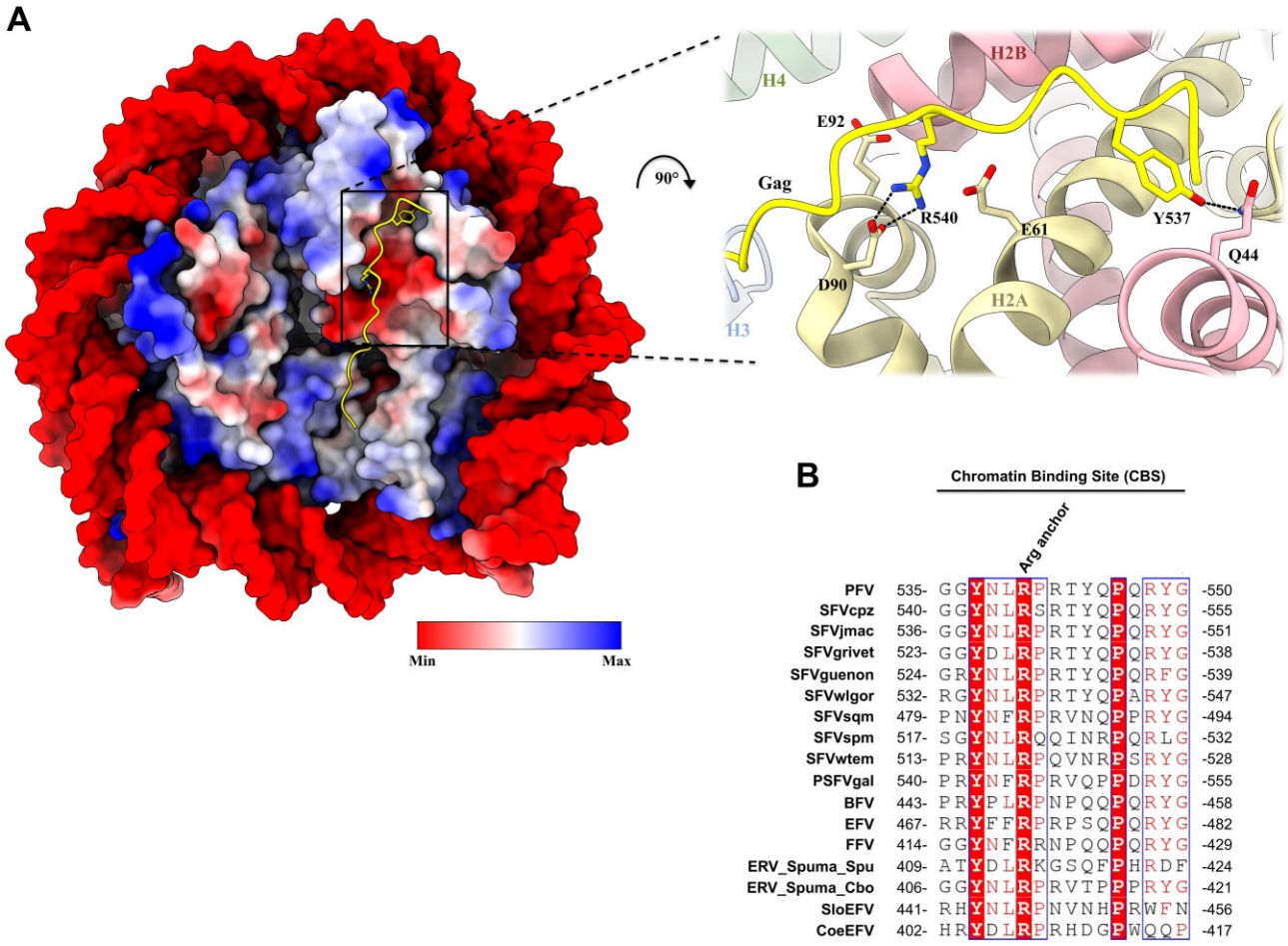

Figure 1. PFV Gag CBS interaction with a human nucleosome. (**A**) Overview of the PFV Gag CBS–nucleosome complex structure shown as a surface representation colored as electrostatic potential (left; database accession code 5MLU). Cartoon representation of the acidic patch engaged by PFV Gag CBS (right). PFV Gag CBS peptide is colored in yellow; histones H2A, H2B, H3, and H4 are shown in pale yellow, red, blue, and green, respectively. (**B**) Amino acid sequence alignment of Gag CBSs. PFV: prototype foamy virus; SFV: simian foamy virus; pve, *Pan troglodytes verus*; mfu, *Macaca fuscata*; cae, *Chlorocebus aethiops*; cni, *Cercopithecus nictitans*; ggo, *Gorilla gorilla gorilla*; ssc, *Saimiri sciureus*; a, *Ateles* species; cja, *Callithrix jacchus*; ocr, *Otolemur crassicaudatus*; BFV, bovine foamy virus; EFV, equine foamy virus; FFV, feline foamy virus; ERV Spuma Spu, endogenous retrovirus Spuma *Sphenodon punctatus*; Cbo, *Ciconia boyciana*; SloEFV, sloth endogenous foamy virus; CoeEFV, Coelacanth endogenous foamy virus. The alignment was performed using ESPript 3.

during the course of mitosis, we infected G2/M-synchronized HT1080 cells with single-round PFV particles encoding Gag WT, R540Q, or Y537Q. Cells were arrested at the G2/M boundary using cyclin-dependent kinase 1 inhibitor RO-3306 [37]. Removal of the molecule by washing allowed the arrested cells to progress into mitosis in a synchronous fashion (Supplementary Figs S1 and S2). To synchronize PFV infection, virus particles were added to G2/M-arrested cells 1 h prior to RO-3306 removal, which induced Gag accumulation at the microtubule organizing complex (MTOC) [38] (Fig. 3). Infected cells were fixed at different time points after G2/M block release, representing different mitotic phases, and stained by immunofluorescence using anti-Gag and anti-Lamin A/C antibodies. Lamin A/C staining was used as a marker for nuclear envelope integrity and chromatin accessibility. The percentage of Gag chromatin occupancy was quantified at each mitotic phase (Fig. 3 and Supplementary Fig. S3). Staining of incoming WT Gag particles showed that following centrosome duplication in prophase, chromatin tethering was concomitant with nuclear envelope breakdown at late prophase/early pro-metaphase (Fig. 3, top panels). The viral proteins decorated cellular chromosomes during further mitotic steps and the nuclei of newly divided interphasic cells. Consistent with previous reports, although PFV Gag R540Q particles accumulated at the MTOC, they were effectively excluded from chromatin at all stages of mitosis and interphasic cells [14, 39, 40] (Fig. 3, middle panels). PFV Gag Y537Q particles displayed a unique phenotype. From the beginning of mitosis and until metaphase, Gag Y537Q phenocopied Gag R540Q behavior, with MTOC retention and exclusion from chromatin. However, Y537Q particles shifted from this chromatin-excluded state to a chromatin-bound state during late mitosis, at telophase (Fig. 3, bottom panels). This unexpected result underscored that despite chromatin juxtaposition after nuclear envelope breakdown, an additional layer of regulation prevented Gag Y537Q–chromatin interactions until the late stages of mitosis. These data showed that in addition to altering nucleosome binding, substitutions of conserved CBS residues can induce a delay in chromatin capture during mitosis.

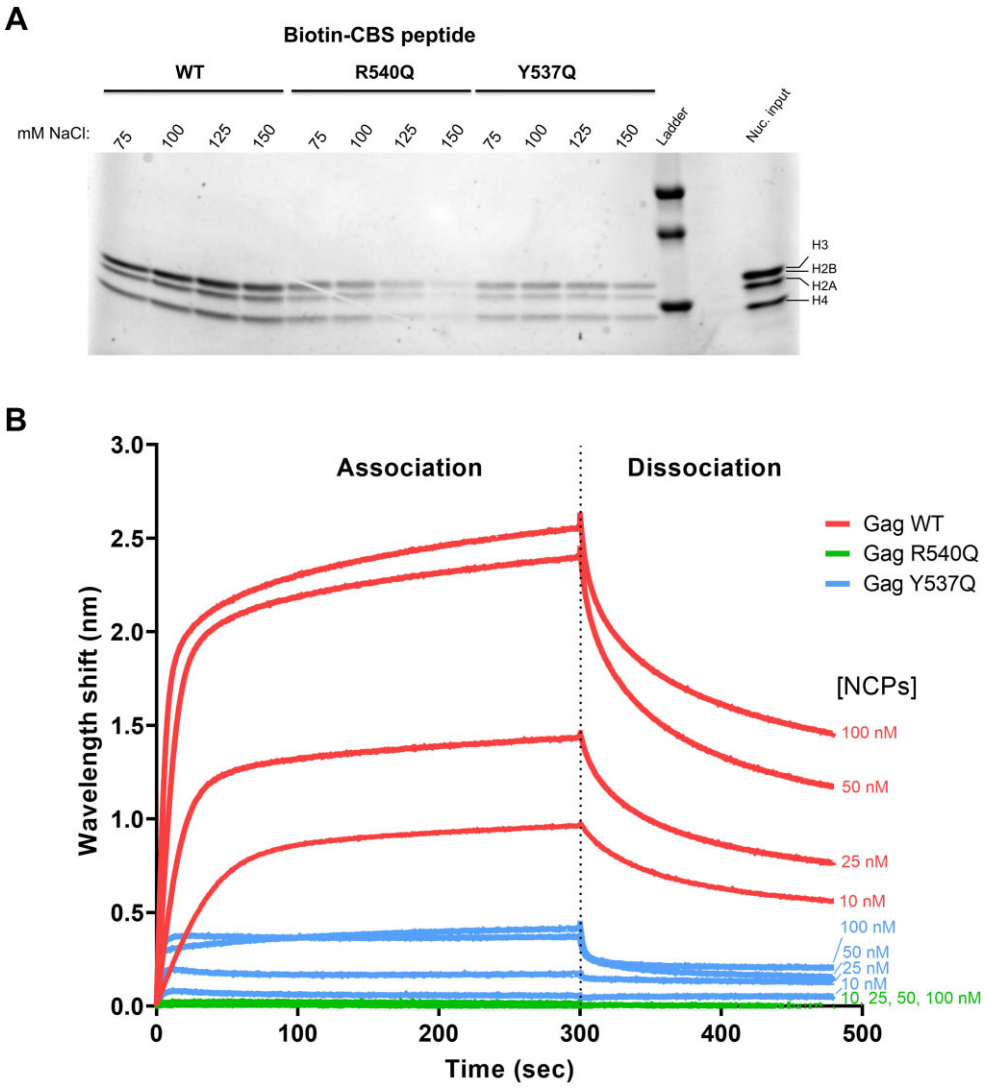

Figure 2. PFV Gag residue Y537 contributes significantly to the interaction with nucleosomes. (**A**) Streptavidin pull-down of recombinant nucleosomes with biotinylated Gag CBS peptides in the presence of 75–150 mM NaCl. (**B**) BLI sensorgram of immobilized Gag CBS peptides and different concentrations of recombinant NCP. The binding intensity (nm) is normalized with a buffer condition without NCP. Results are representative of three independent experiments.

Untimely capture of mitotic chromatin influences PFV fitness

We next investigated the effect of invariant CBS residue substitutions on viral infectivity. WT and CBS mutant PFV particles were purified by ultracentrifugation through 20% sucrose cushions. Viral input used for each transduction was quantified by immunoblotting and subsequently, 1 h post-infection, by real-time PCR for relative viral genome copy number determination (Supplementary Fig. S4A). For an infection-defective control, we used IN active site mutant virus IN-NQ. HT1080 cells were transduced with equal amounts of viral particles and cultured for 6 days before being subjected to flow cytometry to quantify the percentage of GFP-positive cells. As expected, IN-NQ virus was unable to establish a productive infection (Fig. 4A). Consistent with previous results, R540Q led to an ∼40% decrease of GFP-positive cells (Fig. 4A) [14, 40]. Gag Y537Q mutant virus harbored a more moderate, but still significant, ∼25% decrease of infectivity.

As particles containing Gag Y537Q displayed delayed chromatin tethering compared to WT (around 3 h; Fig. 3 and Supplementary Fig. S3), we next measured whether this effected the relative timing of integration. To this end, we synchronously infected HT1080 cells with WT, R540Q, or Y537Q particles and blocked the integration step at different times post-infection using the IN inhibitor DTG. DTG was maintained at 2 μM in the cell growth medium until flow cytometry analysis 6 days post-infection. If the delayed chromatin tethering observed with CBS mutants delayed integration, the kinetics of infection should be differentially sensitive to DTG treatment. As seen in Supplementary Fig. S4B, the integration kinetics of all three viruses were highly similar. This observation suggests that the untimely chromatin tethering observed with PFV Gag CBS substitution mutants did not appreciably affect the timing of integration.

Next, we performed real-time PCR using primers specific to the PFV long terminal repeat (LTR) region to quantify integration efficiency 6 days post-infection. As observed in Fig. 4B, integration was barely detectable for IN-NQ control virus, and infections performed with PFV Gag R540Q and Y537Q mutant particles showed ∼40% and ∼35% decreases from

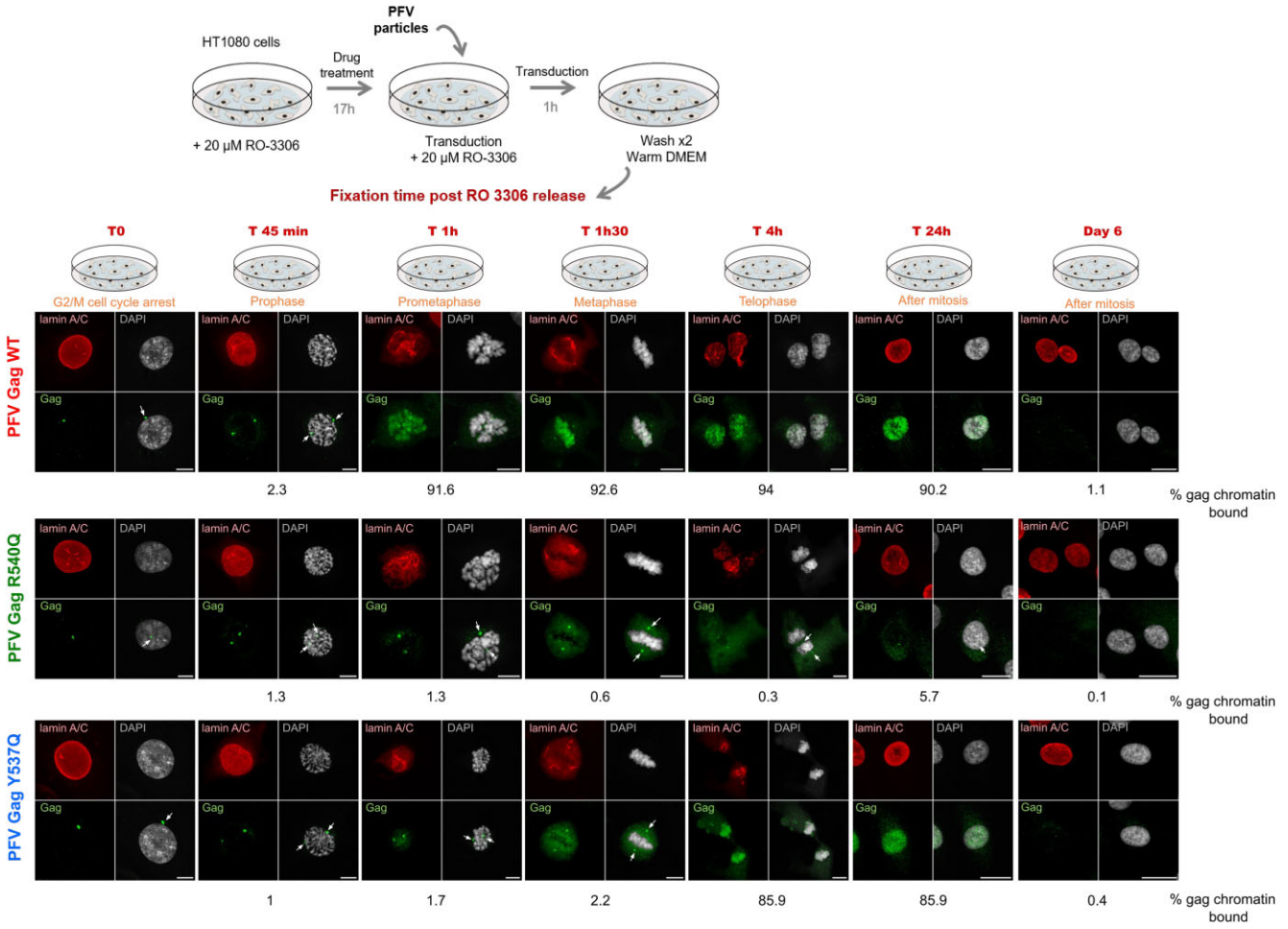

Figure 3. Conserved Gag CBS residues are essential for timely mitotic chromatin capture. Gag localization during PFV infection. G2/M-phase synchronized HT1080 cells were transduced with PFV particles encoding WT, R540Q, or Y537Q Gag and fixed at different time points after drug release, corresponding to different mitotic phases indicated in orange. Gag proteins were detected using polyclonal anti-PFV Gag antiserum (green); the nuclear envelope was stained with anti-Lamin A/C antibodies (red) and cellular DNA with DAPI (gray). White arrows show MTOC accumulation of PFV Gag. Scale bars: 20 µm. Percentages of chromatin-bound Gag are indicated for each mitotic phase. See "Materials and methods" section for detailed information on quantification. Results are representative of those observed across at least five independent experiments.

the WT, respectively. These data reveal an important role for early chromatin tethering by PFV Gag during mitosis to ensure optimal genome capture for subsequent integration.

Y537Q redirects integration to late-replication markers of host chromatin

Our previous results demonstrated that the R540Q substitution led to massive redistribution of integration events into centromeric regions of the genome [14]. We next investigated the effect of the Y537Q variant on integration site selection, comparing the results to previously determined WT and R540Q sites [14] as well as a reference set of *in silico*-selected random integration control (RIC) sites (Supplementary Table S1). Sites of Y537Q integration displayed a unique pattern of proviral distribution (Fig. 5 and Supplementary Table S2). Although maintaining a preference for centromeric regions versus the WT, Y537Q targeted centromeres less robustly than did R540Q ($P = .035$; Supplementary Table S2). In contrast, Y537Q showed the greatest preference for Giemsa-positive cytobands (gp100) and LADs, and was least biased for elements associated with active chromatin, including gene-dense regions, transcriptional activity, and speckle-associated domains (SPADs). While WT PFV integration was enriched near transcriptional start sites (TSSs) and CpG islands, these features were avoided by the Y537Q and R540Q viruses.

Compared to the R540Q mutant, Y537Q integration disfavored gene-dense regions of chromatin ($P = .009$; Supplementary Table S2). To assess the granularity of this difference, we plotted the percentage of integration sites per Mb on each autosomal chromosome, which showed a significant preference for Y537Q to integrate into a subset of human chromosomes (Fig. 6A). Chromosomes 21, 4, 18, 13, and 6 were among the most frequent targets of Y537Q integration (Supplementary Tables S3 and S4). Conversely, chromosomes 22, 19, 17, 15, 16, and 20 were highly avoided for integration. These chromosome clusters differ with respect to replication timing, as chromosomes 22, 20, 19, 17, 16, and 15 are the earliest replicating chromosomes while chromosomes 21, 18, 13, and 4 are comparatively late replicating [41]. To further probe this connection, we stratified chromosomes into three groups based on replication timing, and plotted percent integration per Mb (Fig. 6B). WT and the Gag CBS mutants generally preferred late-replicating as compared to early-replicating chromosomes for integration. However, compared to R540Q, Y537Q targeted early-replicating chro-

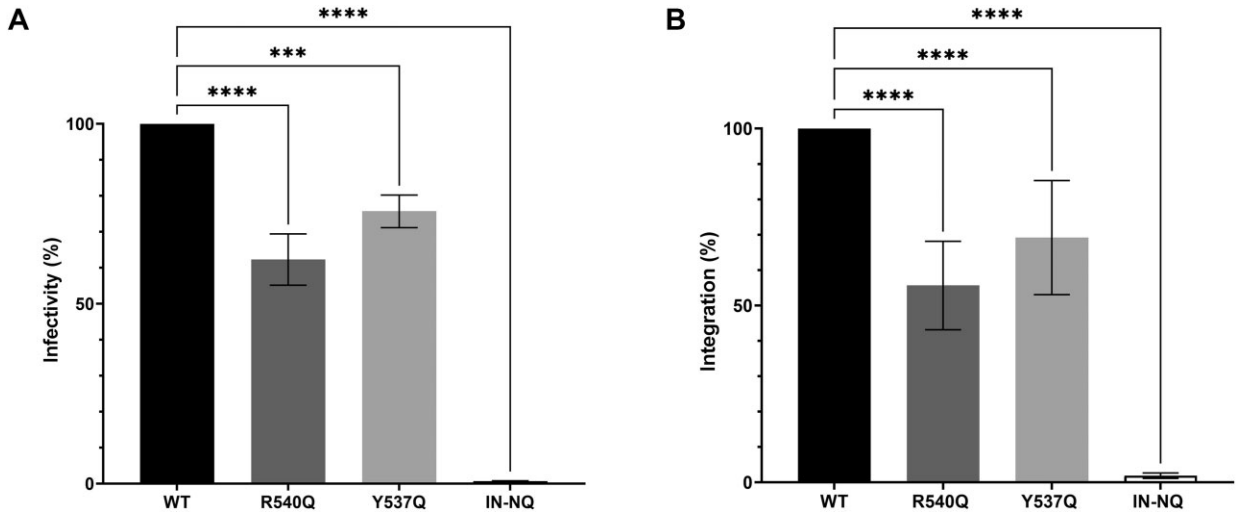

Figure 4. Conserved PFV Gag CBS residues are required for optimal infectivity. (**A**) Six days post-infection, GFP-positive cells were counted by flow cytometry as relative measures of infectivity. Error bars are SDs determined from at least three independent infections; the WT values in each experiment were set to 100%. (**B**) Quantitative PCR of integrated vDNA, 6 days after HT1080 infection, with PFV vector particles carrying WT, R540Q, or Y537Q Gag with WT IN or WT Gag containing virus with catalytically inert D185N/ E221Q IN (IN-NQ). Results are expressed as percentage relative to the WT condition, which was set to 100%. Statistical analyses were performed using the ordinary one-way ANOVA, with Tukey's multiple comparisons tests (***$P < .0005$; ****$P < .0001$).

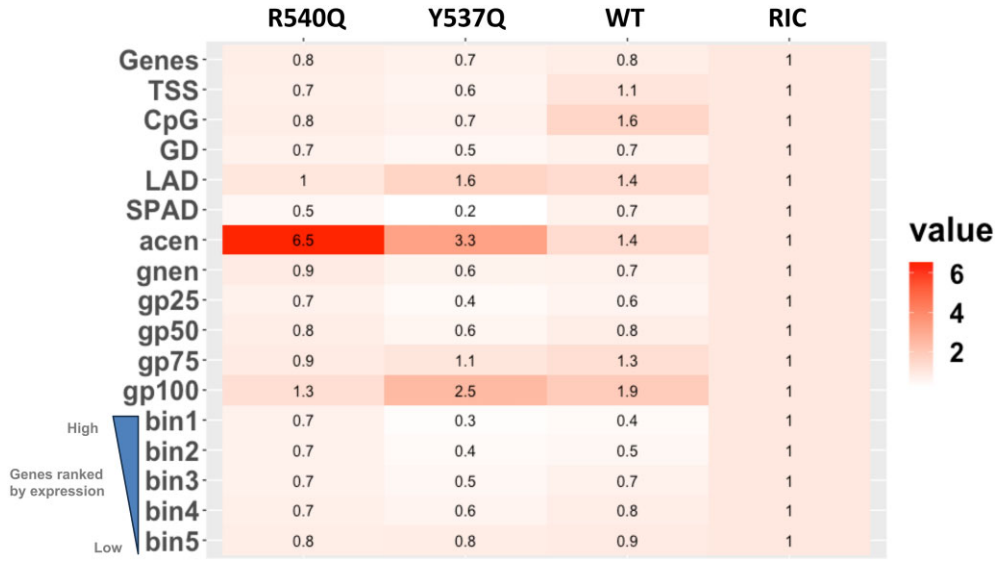

Figure 5. Integration site distributions of WT and Gag CBS mutant viruses. Integration frequencies normalized to *in silico*-calculated RICs are shown as a heatmap. Values >1 (red color) indicate enrichment of PFV sites compared to random, whereas values <1 (white color) represent features avoided by PFV for integration. Genes were divided into five groups based on expression, with bin1 being top-expressed genes. Human cytobands specific to genome build hg38 are shown as acen, gnen, gp25, gp50, gp75, and gp100. TSS, GD, LAD, and SPAD represent transcription start site, gene density (±0.5 Mb), lamina-associated domain, and speckle-associated domain.

mosomes significantly less ($P < 10^{-10}$) and late-replicating chromosomes significantly more ($P < 10^{-10}$) (Fig. 6B and Supplementary Table S5). Despite the difference in integration for various genomic features such as centromeres (Fig. 5), R540Q and WT PFV, moreover, similarly targeted early- and late-replicating chromosomes for integration ($P = .6$ and .9 for early and late-replicating chromosomes, respectively). To independently validate this observation, we correlated chromosomal distributions of RepID occupancy [31] with PFV integration site distributions. As seen in Fig. 6C, chromosomes 22, 19, 17, and 20 were highly enriched for RepID, whereas, chromosomes 21, 13, 4, and 18 were comparatively RepID-poor. Consistently, we observed a significant inverse correlation between RepID-enriched chromosomes and Y537Q integration sites ($R^2 = 0.66$; R^2 for WT and R540Q = 0.28 and 0.12, respectively) (Fig. 6D and Supplementary Table S6). The seven chromosomes least enriched for RepID were most frequently targeted by Y537Q, whereas RepID-enriched chromosomes were less targeted by Y537Q compared to WT and R540Q, confirming the integration bias of Y537Q for late-replicating chromosomes (Fig. 6C and D).

We next correlated RepID occupancy across human genes, and identified that genes devoid of RepID sites accounted for the overall similar preference for Y537Q and R540Q to tar-

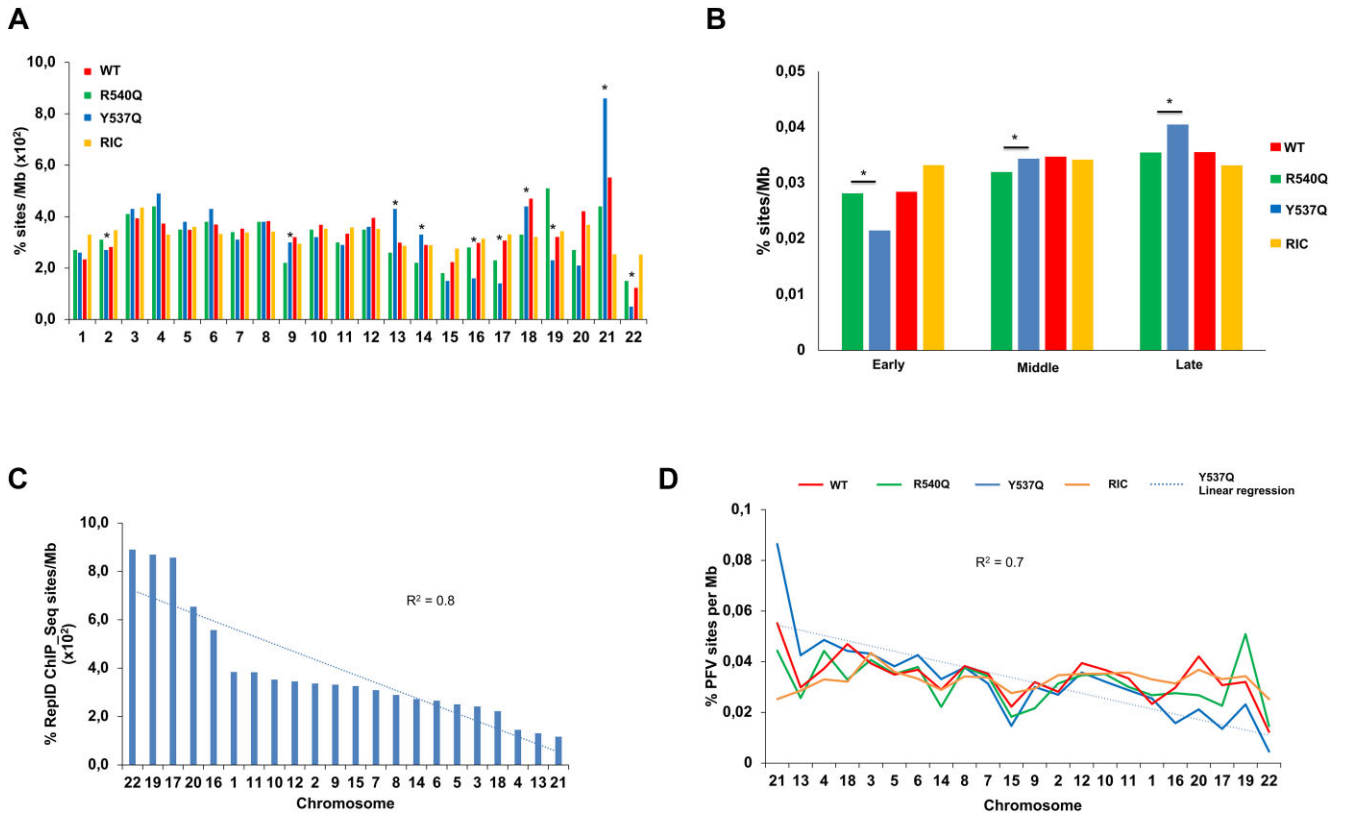

Figure 6. Chromosomal distributions of PFV proviruses. (**A**) PFV integration sites % per Mb (*Y*-axis) of indicated human chromosomes (*X*-axis) are shown for R540Q and Y537Q viruses along with WT PFV and RIC. Significant differences in chromosomal targeting between R540Q and Y537Q is shown (Fisher's exact test; $P < .05$). (**B**) PFV integration % per Mb for three chromosomal groups based on replication timing: early, middle, and late replicating (*X*-axis). PFV integration per Mb for each group is shown (*$P < .05$ between R450Q and Y537Q; Fisher's exact test). (**C**) Chromosomal distribution of RepID ChIP-seq sites per Mb. (**D**) Correlation between chromosomal distribution of RepID binding sites per Mb and % PFV integration sites per Mb.

get genes for integration (Fig. 5) ($P = .08$) (Supplementary Fig. S5C and Supplementary Table S7). In contrast, RepID-associated genes were significantly less targeted by Y537Q for integration ($P < 10^{-10}$) (Supplementary Fig. S5B and Supplementary Table S7). Compared to the mutants, WT PFV differentially targeted RepID-associated genes, yet targeted genes devoid of RepID sites similarly as the CBS Gag mutants for integration (Supplementary Fig. S5B and C). Consistent with the reduced preference for Y537Q to target early-replicating chromosomes for integration, Y537Q integrated significantly less frequently into ±2.5-kb regions of RepID sites than did WT and R540Q ($P < 10^{-10}$) (Supplementary Fig. S5A and Supplementary Table S7).

We next sought to independently verify the unique pattern of Y537Q integration targeting. The human genome can be represented as 10 spatial position inference of the nuclear genome (SPIN) states [32], which are radially distributed from the nuclear center (Speckles SPIN state) to the periphery (Lamina state). Correlating WT, R540Q, and Y537Q PFV integration sites with SPIN states indicated that all three viruses disfavored integration within the seven innermost states (Speckles, Act1, Act2, Act3, Repr1, Repr2, and Lm1), while the three outermost SPIN states (Lm2, Lamina_Like, and Lamina) were significantly more targeted than random (Supplementary Fig. S6 and Supplementary Table S8). Notably, Y537Q integration positively correlated with SPIN states from the center to the periphery ($R^2 = 0.6$) while WT ($R^2 = 0.3$) and R540Q ($R^2 = 0.2$) exhibited integration patterns more similar to the RIC ($R^2 = 0.3$) (Supplementary Fig. S6). These findings indicate that the Y537Q PFV mutant shifts integration from central gene-dense genomic regions to more peripheral regions of the genome. Since LADs, which represent late-replicating genomic regions, are predominantly in the Lamina state, these findings support the results presented in Fig. 6.

Differential gene targeting by PFV Gag CBS mutant viruses

Because Y537Q Gag binding to mitotic chromatin was significantly delayed compared to the WT (Fig. 3 and Supplementary Fig. S3), we next investigated the connection between mitotic chromatin dynamics and PFV integration. To examine chromatin state transitions, we analyzed published data on mitotic-specific transcription [30], which reported gene expression levels at different time points ($t = 0$, 40, 80, 105, 165, and 300 min) after the release of nocodazole-induced mitotic arrest. We compared the expression of genes at $t = 105$ min to their expression at three earlier time points, $t = 0$, 40, and 80 min. Genes were identified as mitotic-specific at $t = 0$ (early), $t = 40$ (middle), and $t = 80$ (late mitosis) if their expression at these time points was at least 1.5-fold higher than that at $t = 105$ min. These mitotic-specific genes were then ranked by transcriptional activity and then halved based on expression level. Using these six gene sets, we assessed their enrichment for early-, middle-, or late-

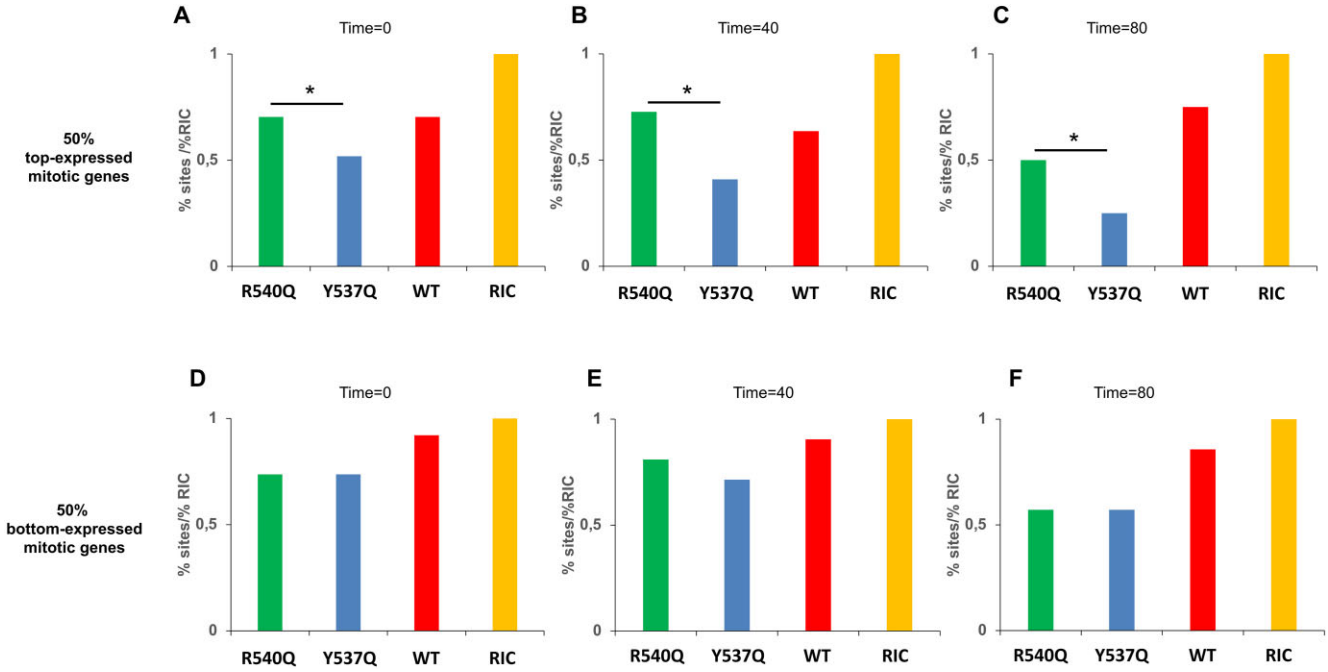

Figure 7. PFV integration sites within mitotic expressed genes. Mitotic genes were classified at 0 (**A**, **D**), 40 (**B**, **E**), and 80 (**C**, **F**) min if the expression of the gene was ≥1.5 times its expression at 105 min from release of mitotic arrest. PFV genic sites (%) are shown for 50% top-expressed in panels (A)–(C) and 50% bottom-expressed mitotic genes in panels (D)–(F). *, Significant difference in targeting between R540Q and Y537Q (Fisher's exact test; $P < .05$).

replicating chromosomes (referred to as early-, middle-, and late-replicating genes) in top 50% versus bottom 50% genes at each time point. This analysis revealed that well-expressed genes at $t = 0$ min and $t = 40$ min were significantly enriched for early replication ($P < .00001$; Fisher's exact test) (Supplementary Table S9). However, by $t = 80$ min (late mitosis), this enrichment was lost ($P = .08$). Additionally, we observed that the bottom half of expressed genes were enriched for late replication at $t = 0$ min, $t = 40$ min and $t = 80$ min ($P < .01$; Fisher's exact test). These findings indicate that early-replicating genes are preferentially expressed at $t = 0$ min and $t = 40$ min, while late-replicating genes are underrepresented in top 50% genes. As mitosis progresses, these enrichment patterns are lost, with early- and late-replicating genes becoming more randomly distributed (or distributed as per their expected genome frequencies) between highly and less expressed gene groups.

Our results demonstrated that the Y537Q mutant targets early-replicating chromosomes significantly less than the WT and R540Q mutant, while preferentially targeting late-replicating chromosomes (Fig. 6B). Moreover, Y537Q and R540Q mutants differentially targeted RepID-associated genes (early-replicating) versus non-associated genes (late-replicating) (Supplementary Fig. S5B and C). Given the distinct targeting patterns of these mutants with respect to replication timing, we next investigated their preferences for transcriptional activity. Because the upper 50% of expressed genes at $t = 0$ min and $t = 40$ min were predominantly early-replicating (Supplementary Table S9), we hypothesized that these genes would be differentially targeted by Y537Q versus R540Q for integration, while the lower half of expressed genes would be similarly targeted. As expected, compared to R540Q, Y537Q disfavored integration into the top 50% of expressed genes (Fig. 7A–C and Supplementary Table S10). Reciprocally, both mutants similarly targeted comparatively poorly expressed genes across time points (Fig. 7D–F).

WT PFV Gag but not CBS mutant Y537Q displaces the H4 tail from the acidic patch

The phenotype observed for Y537Q chromatin engagement during mitosis (Fig. 3, bottom panel) prompted us to investigate the mechanisms underlying its delayed access. During mitosis, chromatin condensation increases until the end of metaphase [42]. In late anaphase and telophase, mitotic chromosomes decondense to re-establish interphase chromatin radial distribution of chromosome domains [42, 43]. The H2A–H2B acidic patch Gag docking station is an important determinant for chromatin compaction by hosting the neighboring nucleosome amino-terminal H4 tail [44–47]. In such condensed early mitotic chromatin, nucleosome acidic patches are preferentially occupied by H4 tails. To explain the Gag Y537Q phenotype, we hypothesized that depending on H2A–H2B acidic patch accessibility during the course of mitosis, chromatin segues from a condensed refractory state to a more open, binding-permissive state. In such a scenario, WT PFV Gag has the ability to compete for the H4 tail–acidic patch interaction, explaining its early chromatin binding mode during virus infection, while Gag Y537Q requires more opened chromatin with comparatively accessible acidic patches. To test our hypothesis, we performed BLI competition experiments using immobilized PFV Gag CBS peptides challenged with NCP saturated with H4 tails to mimic occupied acidic patches from condensed early mitotic chromatin. We first monitored binding of WT H4 tail (H4 WT) versus nucleosome interaction deficient mutant (H4 mut) peptides to purified NCPs. WT H4 tails, but not the mutated versions, efficiently interacted with recombinant NCPs (Supplementary Fig. S7). Next, we probed

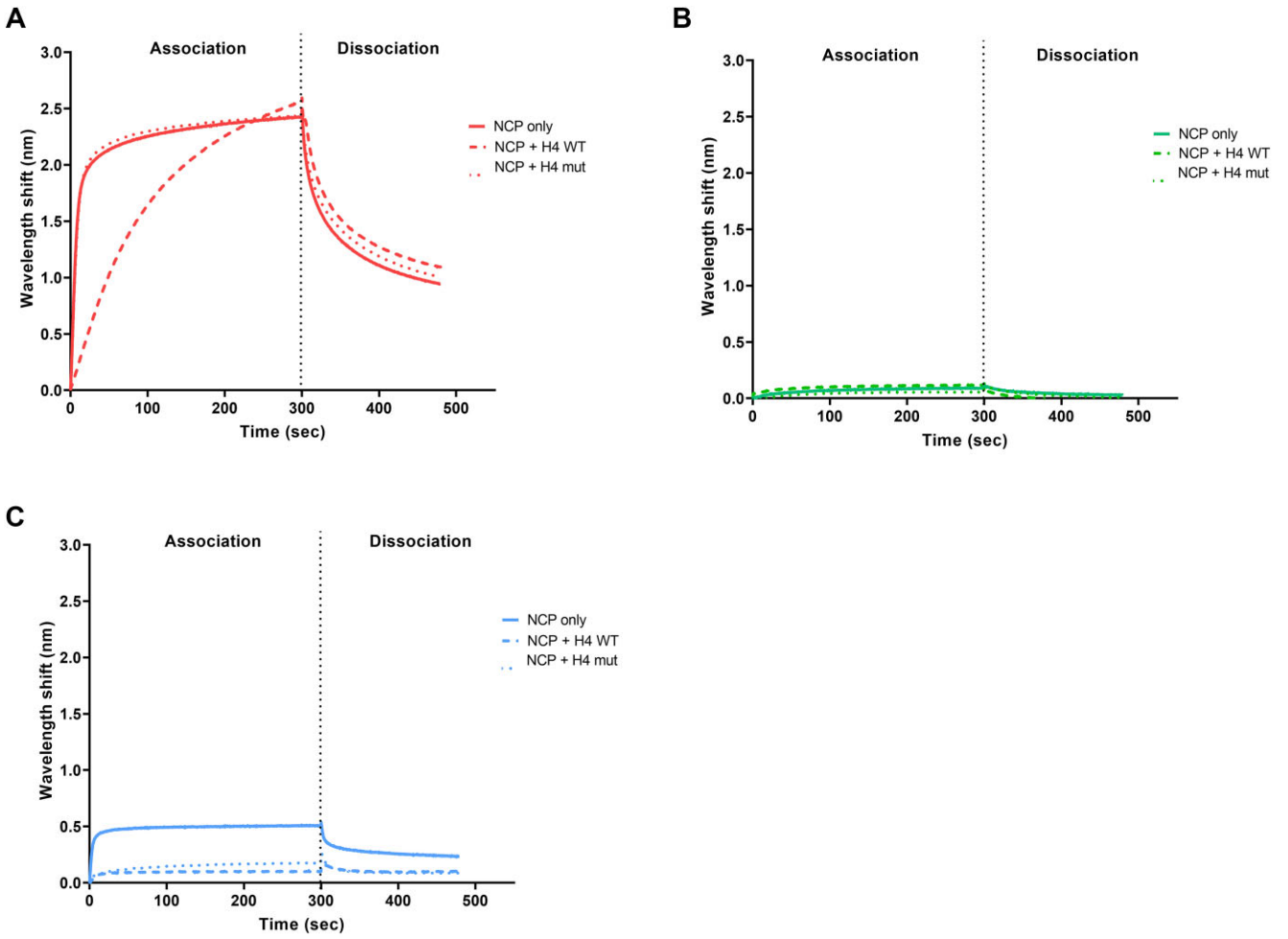

Figure 8. Interaction of the H4 tail to the nucleosome acidic patch prevents Gag Y537Q binding. BLI sensorgram of free nucleosomes (NCP, plain line), saturated with WT H4 tail (residues 2–24) (dashed line) or H4 mut (triple alanine substitution) (dotted line) binding to immobilized (**A**) WT Gag (red), (**B**) R540Q Gag (green), and (**C**) Y537Q Gag (blue) peptides. Binding intensity (nm) was normalized to conditions without NCP. The mean of two independent experiments is plotted.

PFV Gag peptide capacity to compete with the H4 tail for H2A–H2B acidic patch binding. As seen in Fig. 8A, WT PFV Gag CBS interaction kinetics with NCPs under saturating concentration of WT H4 tails, but not the H4 mut tails, showed a modified, slower association curve. Under these competition conditions, the interaction reached the same level as without H4 tails, and was consistent with displacement events in favor of the PFV Gag CBS. The same experiment was performed with immobilized PFV Gag R540Q (Fig. 8B), which recapitulated the results observed in Fig. 2B, namely no interaction with the NCP. With CBS peptide Y537Q, the results in Fig. 8C showed that PFV Gag Y537Q was unable to effectively compete for H2A–H2B acidic patch binding with nucleosome saturated by H4 WT or H4 mut (as seen in Supplementary Fig. S7, H4 mut peptide retains some residual binding that, in excess, is sufficient to prevent Gag Y537Q binding). These BLI experiments highlighted that WT PFV Gag CBS peptides retain chromatin binding under conditions of excess H2A–H2B acidic patch interacting competitor (H4 tail). Conversely, binding capacity of PFV Gag Y537Q CBS peptides for the nucleosomes was drastically reduced by the presence of the H4 tail. These data are consistent with the hypothesis that H4-occupied acidic patches in condensed mitotic chromatin restrict Gag Y537Q binding.

Discussion

Here we show that the PFV Gag CBS harbors invariant residues crucial for H2A–H2B acidic patch engagement and integration site selection. In addition to the previously characterized arginine anchor motif R540, we identified a highly conserved Y537 residue contributing to the interaction with nucleosomes. Although not essential for chromatin binding, substituting this tyrosine for glutamine decreased NCP capture ∼5-fold (Fig. 2B). These results are consistent with previous observations [48, 49] and highlight the crucial role of CBS Gag residues in interacting with the nucleosome acidic patch. Nucleosome binding is a prerequisite for many cellular factors to fulfill chromatin transactions. A recent comprehensive study showed that >50% of nucleosome interactions are mediated by the acidic patch [50]. The plethora of nucleosome complex structures solved by cryo-electron microscopy provided an extensive source of molecular information governing acidic patch engagement. They revealed a strong conservation of the arginine anchor motif but also illuminate the variety of secondary contacts within the acidic patch [34, 51]. As seen with Gag Y537Q, such secondary contacts may tune the affinity requirements for chromatin interactions. R540Q mutation ablates Gag–chromatin interaction [14] (Fig. 2), making the virus to integrate into centromeres, positioned close to cen-

trosomes, where viral capsids accumulate. Conversely, the intermediate phenotype of Y537Q makes this mutation more informative about the functional implications of FV Gag–chromatin interaction. Additionally, it would be of interest to further investigate how potential post-translational modifications of Arg [49] and Tyr [52] may regulate the strength of nucleosome tethering and, consequently, impact downstream viral processes.

Akin to most orthoretroviruses, FVs cannot infect resting cells and require nuclear envelope breakdown during mitosis to access chromatin [53]. We tracked PFV Gag proteins after infecting cell cycle synchronized cells with viral particles harboring CBS amino acid substitutions R540Q or Y537Q. WT particles showed practically immediate chromatin tethering upon nuclear envelope breakdown. Altering nucleosome binding with the Y537Q substitution unexpectedly delayed chromosome capture until telophase. We provided biochemical evidence that Gag Y537Q's incapacity to bind early mitotic chromosomes is likely due to its inability to displace the H4 tail from condensed chromatin acidic patches. Indeed, several reports showed a major role for the H4 tail–acidic patch interaction in high order chromatin structure [54, 55]. Additionally, disruption of this interaction, such as in the case of pioneer transcription factors, leads to a destabilization of chromatin packing, facilitating its opening for subsequent DNA transactions [56]. It will be of interest to determine whether PFV Gag possesses the capacity to alter local chromatin structure by evicting the H4 tail from the acidic patch and the potential role in viral and cellular functions [51].

Accessing and persisting in the nuclear compartment is a challenge for many viruses. The nuclear envelope represents an impassable barrier for several viruses that rely on mitosis to access chromatin [57]. Here we confirmed the important role of PFV Gag tethering to chromatin. Indeed, affecting Gag's capacity to engage chromatin provoked a significant decrease of viral infectivity, with a decrease of integrated viral DNA. In addition, infections with Gag CBS variants induced a redistribution of integration sites along the host genome with a marked preference of the Gag Y573Q virus to target late-replicating chromosomes (Fig. 6 and Supplementary Fig. S6). During telophase, chromatin decondensation is triggered along with post-mitotic radial rearrangements of chromosome domains [43, 58, 59]. Compared to the buried, inner nucleus and less accessible early-replicating domains, late-replicating chromosomes are distributed at the periphery [60]. These peripheral, late-replicating chromosomal regions may serve as a selective binding platform for Y537Q Gag, linking our immunofluorescence observations (Fig. 3 and Supplementary Fig. S3) and integration site selection analyses (Fig. 6).

Integration site selection is a common feature of retroviruses although each genus evolved specific mechanisms to select their insertion loci. However, we note that the Y357Q phenotype (Supplementary Fig. S6) resembles the behavior of the CPSF6 binding-deficient HIV-1 N74D capsid mutant virus, which shifts HIV-1 integration sites from gene-dense, centrally located SPAD/speckle-enriched chromosomes to gene-poor, LAD/Lamina-enriched chromosomes [17, 18, 24]. We furthermore note that a recent study has described SPADs as early-replicating chromosomal regions [59]. Because previous research indicated that speckle depletion did not affect HIV-1 integration into SPADs [61], it seems that replication timing, in addition to spatial organization of chromosomes, may play a role in lentiviral DNA integration targeting. We plan in the future to further explore the relationship between DNA replication timing and orthoretroviral DNA integration.

We previously described the PFV Gag CBS as a pan-nucleosome binder important for maintaining integration site distribution [14]. Herein we revealed that the observed integration site selection phenotype of CBS variants is the consequence of delayed chromatin capture and the spatial chromosomal reorganization along the course of mitosis that, depending on the mitotic stage, exposes different chromosomes and genes to PFV integration complexes. In light with the correlation between tethering timing during mitosis and integration selectivity, it is tempting to speculate a potential opportunistic mechanism of spumaretroviral integration site selection; Gag-containing pre-integration complexes will interact with the first suitable and available nucleosomes to dictate eventual integration location. To best succeed, FVs evolved a strong chromatin binding capacity in order to capture highly condensed chromatin early in mitosis. This ensures optimal chromatin retention, integration, and viral infectivity. Harnessing this intrinsic, unique chromatin binding capacity of spumaretroviral Gag might constitute a promising starting platform for the development of targeting-tunable FV-based vectors in gene therapy.

Acknowledgements

We would like to thank Nicolas Landrein for his technical support with image quantification.

Author contributions: Floriane Lagadec (Conceptualization, Data curation, Formal analysis, Investigation, Methodology, Visualization, Writing—original draft, Writing—review & editing), Parmit K. Singh (Conceptualization, Data curation, Formal analysis, Investigation, Methodology, Visualization, Writing—original draft, Writing—review & editing), Christina Calmels (Formal analysis), Delphine Lapaillerie (Formal analysis), Dirk Lindemann (Resources, Writing—review & editing), Vincent Parissi (Conceptualization, Funding acquisition, Writing—review and editing), Peter Cherepanov (Conceptualization, Resources, Writing—review & editing), Alan N. Engelman (Conceptualization, Funding acquisition, Validation, Writing—review & editing), and Paul Lesbats (Conceptualization, Data curation, Formal analysis, Funding acquisition, Investigation, Methodology, Project administration, Supervision, Validation, Visualization, Writing—original draft, Writing—review & editing).

Supplementary data

Supplementary data is available at NAR online.

Conflict of interest

None declared.

Funding

This work was supported by the French National Research Agency (ANR) under the Young Researcher Grant (ANR-19-CE15-000 to P.L.), by the Fondation pour la Recherche Médicale (FRM—Labélisation équipe FRM, EQU202303016283) and by grants from the US National Institutes of Health

(R37AI039394 and R01AI052014 to A.N.E.). Funding to pay the Open Access publication charges for this article was provided by CNRS funding and FRM funding.

Data availability

The BED files associated with PFV integration sites are available at https://dataverse.harvard.edu/dataset.xhtml?persistentId=doi:10.7910/DVN/PP9APV. The hg19 RefSeq genes specific to mitotic time points 0, 40, and 80 min are available at https://dataverse.harvard.edu/dataset.xhtml?persistentId=doi:10.7910/DVN/RFKDMH.

References

1. Rethwilm A, Bodem J. Evolution of foamy viruses: the most ancient of all retroviruses. *Viruses* 2013;**5**:2349–74. https://doi.org/10.3390/v5102349
2. Pinto-Santini DM, Stenbak CR, Linial ML. Foamy virus zoonotic infections. *Retrovirology* 2017;**14**:55. https://doi.org/10.1186/s12977-017-0379-9
3. Betsem E, Rua R, Tortevoye P *et al.* Frequent and recent human acquisition of simian foamy viruses through apes' bites in Central Africa. *PLoS Pathog* 2011;**7**:e1002306. https://doi.org/10.1371/journal.ppat.1002306
4. Buseyne F, Betsem E, Montange T *et al.* Clinical signs and blood test results among humans infected with zoonotic simian foamy virus: a case-control study. *J Infect Dis* 2018;**218**:144–51.
5. Gessain A, Montange T, Betsem E *et al.* Case-control study of the immune status of humans infected with zoonotic gorilla simian foamy viruses. *J Infect Dis* 2020;**221**:1724–33. https://doi.org/10.1093/infdis/jiz660
6. Simantirakis E, Tsironis I, Vassilopoulos G. FV vectors as alternative gene vehicles for gene transfer in HSCs. *Viruses* 2020;**12**:332. https://doi.org/10.3390/v12030332
7. Hare S, Gupta SS, Valkov E *et al.* Retroviral intasome assembly and inhibition of DNA strand transfer. *Nature* 2010;**464**:232–6. https://doi.org/10.1038/nature08784
8. Maertens GN, Hare S, Cherepanov P. The mechanism of retroviral integration from X-ray structures of its key intermediates. *Nature* 2010;**468**:326–9. https://doi.org/10.1038/nature09517
9. Lesbats P, Engelman AN, Cherepanov P. Retroviral DNA integration. *Chem Rev* 2016;**116**:12730–57. https://doi.org/10.1021/acs.chemrev.6b00125
10. Jordan A, Defechereux P, Verdin E. The site of HIV-1 integration in the human genome determines basal transcriptional activity and response to Tat transactivation. *EMBO J* 2001;**20**:1726–38. https://doi.org/10.1093/emboj/20.7.1726
11. Janssens J, De Wit F, Parveen N *et al.* Single-cell imaging shows that the transcriptional state of the HIV-1 provirus and its reactivation potential depend on the integration site. *mBio* 2022;**13**:e0000722. https://doi.org/10.1128/mbio.00007-22
12. Sultana T, Zamborlini A, Cristofari G *et al.* Integration site selection by retroviruses and transposable elements in eukaryotes. *Nat Rev Genet* 2017;**18**:292–308. https://doi.org/10.1038/nrg.2017.7
13. Maskell DP, Renault L, Serrao E *et al.* Structural basis for retroviral integration into nucleosomes. *Nature* 2015;**523**:366–9. https://doi.org/10.1038/nature14495
14. Lesbats P, Serrao E, Maskell DP *et al.* Structural basis for spumavirus GAG tethering to chromatin. *Proc Natl Acad Sci USA* 2017;**114**:5509–14. https://doi.org/10.1073/pnas.1621159114
15. Schroder AR, Shinn P, Chen H *et al.* HIV-1 integration in the human genome favors active genes and local hotspots. *Cell* 2002;**110**:521–9. https://doi.org/10.1016/S0092-8674(02)00864-4
16. Singh PK, Plumb MR, Ferris AL *et al.* LEDGF/p75 interacts with mRNA splicing factors and targets HIV-1 integration to highly spliced genes. *Genes Dev* 2015;**29**:2287–97. https://doi.org/10.1101/gad.267609.115
17. Francis AC, Marin M, Singh PK *et al.* HIV-1 replication complexes accumulate in nuclear speckles and integrate into speckle-associated genomic domains. *Nat Commun* 2020;**11**:3505. https://doi.org/10.1038/s41467-020-17256-8
18. Singh PK, Bedwell GJ, Engelman AN. Spatial and genomic correlates of HIV-1 integration site targeting. *Cells* 2022;**11**:655. https://doi.org/10.3390/cells11040655
19. Cherepanov P, Maertens G, Proost P *et al.* HIV-1 integrase forms stable tetramers and associates with LEDGF/p75 protein in human cells. *J Biol Chem* 2003;**278**:372–81. https://doi.org/10.1074/jbc.M209278200
20. Shun MC, Raghavendra NK, Vandegraaff N *et al.* LEDGF/p75 functions downstream from preintegration complex formation to effect gene-specific HIV-1 integration. *Genes Dev* 2007;**21**:1767–78.https://doi.org/10.1101/gad.1565107
21. Ciuffi A, Llano M, Poeschla E *et al.* A role for LEDGF/p75 in targeting HIV DNA integration. *Nat Med* 2005;**11**:1287–9. https://doi.org/10.1038/nm1329
22. Lee K, Ambrose Z, Martin TD *et al.* Flexible use of nuclear import pathways by HIV-1. *Cell Host Microbe* 2010;**7**:221–33. https://doi.org/10.1016/j.chom.2010.02.007
23. Schaller T, Ocwieja KE, Rasaiyaah J *et al.* HIV-1 capsid–cyclophilin interactions determine nuclear import pathway, integration targeting and replication efficiency. *PLoS Pathog* 2011;7:e1002439. https://doi.org/10.1371/journal.ppat.1002439
24. Sowd GA, Serrao E, Wang H *et al.* A critical role for alternative polyadenylation factor CPSF6 in targeting HIV-1 integration to transcriptionally active chromatin. *Proc Natl Acad Sci USA* 2016;**113**:E1054–63. https://doi.org/10.1073/pnas.1524213113
25. Lowary PT, Widom J. New DNA sequence rules for high affinity binding to histone octamer and sequence-directed nucleosome positioning. *J Mol Biol* 1998;**276**:19–42. https://doi.org/10.1006/jmbi.1997.1494
26. Munz CM, Kreher H, Erdbeer A *et al.* Efficient production of inhibitor-free foamy virus glycoprotein-containing retroviral vectors by proteoglycan-deficient packaging cells. *Mol Ther Methods Clin Dev* 2022;**26**:394–412. https://doi.org/10.1016/j.omtm.2022.07.004
27. Hamann MV, Stanke N, Müllers E *et al.* Efficient transient genetic manipulation *in vitro* and *in vivo* by prototype foamy virus-mediated nonviral RNA transfer. *Mol Ther* 2014;**22**:1460–71. https://doi.org/10.1038/mt.2014.82
28. Stange A, Lüftenegger D, Reh J *et al.* Subviral particle release determinants of prototype foamy virus. *J Virol* 2008;**82**:9858–69. https://doi.org/10.1128/JVI.00949-08
29. Sweeney NP, Meng J, Patterson H *et al.* Delivery of large transgene cassettes by foamy virus vector. *Sci Rep* 2017;**7**:8085. https://doi.org/10.1038/s41598-017-08312-3
30. Palozola KC, Donahue G, Liu H *et al.* Mitotic transcription and waves of gene reactivation during mitotic exit. *Science* 2017;**358**:119–22. https://doi.org/10.1126/science.aal4671
31. Zhang Y, Huang L, Fu H *et al.* A replicator-specific binding protein essential for site-specific initiation of DNA replication in mammalian cells. *Nat Commun* 2016;**7**:11748. https://doi.org/10.1038/ncomms11748
32. Wang Y, Zhang Y, Zhang R *et al.* SPIN reveals genome-wide landscape of nuclear compartmentalization. *Genome Biol* 2021;**22**:36. https://doi.org/10.1186/s13059-020-02253-3
33. Quinlan AR, Hall IM. BEDTools: a flexible suite of utilities for comparing genomic features. *Bioinformatics* 2010;**26**:841–2. https://doi.org/10.1093/bioinformatics/btq033
34. McGinty RK, Tan S. Principles of nucleosome recognition by chromatin factors and enzymes. *Curr Opin Struct Biol* 2021;**71**:16–26. https://doi.org/10.1016/j.sbi.2021.05.006
35. Robert X, Gouet P. Deciphering key features in protein structures with the new ENDscript server. *Nucleic Acids Res* 2014;**42**:W320–4. https://doi.org/10.1093/nar/gku316

36. Bieniasz PD, Weiss RA, McClure MO. Cell cycle dependence of foamy retrovirus infection. *J Virol* 1995;**69**:7295–9. https://doi.org/10.1128/jvi.69.11.7295-7299.1995
37. Vassilev LT, Tovar C, Chen S *et al.* Selective small-molecule inhibitor reveals critical mitotic functions of human CDK1. *Proc Natl Acad Sci USA* 2006;**103**:10660–5. https://doi.org/10.1073/pnas.0600447103
38. Lehmann-Che J, Renault N, Giron ML *et al.* Centrosomal latency of incoming foamy viruses in resting cells. *PLoS Pathog* 2007;**3**:e74. https://doi.org/10.1371/journal.ppat.0030074
39. Tobaly-Tapiero J, Bittoun P, Lehmann-Che J *et al.* Chromatin tethering of incoming foamy virus by the structural Gag protein. *Traffic* 2008;**9**:1717–27. https://doi.org/10.1111/j.1600-0854.2008.00792.x
40. Müllers E, Stirnnagel K, Kaulfuss S *et al.* Prototype foamy virus gag nuclear localization: a novel pathway among retroviruses. *J Virol* 2011;**85**:9276–85. https://doi.org/10.1128/JVI.00663-11
41. Woodfine K, F H, Dm B *et al.* Replication timing of the human genome. *Hum Mol Genet* 2004;**13**:575. https://doi.org/10.1093/hmg/ddh058
42. Antonin W, Neumann H. Chromosome condensation and decondensation during mitosis. *Curr Opin Cell Biol* 2016;**40**:15–22. https://doi.org/10.1016/j.ceb.2016.01.013
43. Gerlich D, Beaudouin J, Kalbfuss B *et al.* Global chromosome positions are transmitted through mitosis in mammalian cells. *Cell* 2003;**112**:751–64. https://doi.org/10.1016/S0092-8674(03)00189-2
44. Dorigo B, Schalch T, Bystricky K *et al.* Chromatin fiber folding: requirement for the histone H4 N-terminal tail. *J Mol Biol* 2003;**327**:85–96. https://doi.org/10.1016/S0022-2836(03)00025-1
45. Song F, Chen P, Sun D *et al.* Cryo-EM study of the chromatin fiber reveals a double helix twisted by tetranucleosomal units. *Science* 2014;**344**:376–80. https://doi.org/10.1126/science.1251413
46. Wakamori M, Fujii Y, Suka N *et al.* Intra- and inter-nucleosomal interactions of the histone H4 tail revealed with a human nucleosome core particle with genetically-incorporated H4 tetra-acetylation. *Sci Rep* 2015;**5**:17204. https://doi.org/10.1038/srep17204
47. Chen Q, Yang R, Korolev N *et al.* Regulation of nucleosome stacking and chromatin compaction by the histone H4 N-terminal tail–H2A acidic patch interaction. *J Mol Biol* 2017;**429**:2075–92. https://doi.org/10.1016/j.jmb.2017.03.016
48. Wei G, Kehl T, Bao Q *et al.* The chromatin binding domain, including the QPQRYG motif, of feline foamy virus Gag is required for viral DNA integration and nuclear accumulation of Gag and the viral genome. *Virology* 2018;**524**:56–68. https://doi.org/10.1016/j.virol.2018.08.007
49. Paris J, Tobaly-Tapiero J, Giron M-L *et al.* The invariant arginine within the chromatin-binding motif regulates both nucleolar localization and chromatin binding of foamy virus Gag. *Retrovirology* 2018;**15**:48. https://doi.org/10.1186/s12977-018-0428-z
50. Skrajna A, Goldfarb D, Kedziora KM *et al.* Comprehensive nucleosome interactome screen establishes fundamental principles of nucleosome binding. *Nucleic Acids Res* 2020;**48**:9415–32. https://doi.org/10.1093/nar/gkaa544
51. Lagadec F, Parissi V, Lesbats P. Targeting the nucleosome acidic patch by viral proteins: two birds with one stone? *mBio* 2022;**13**:e0173321. https://doi.org/10.1128/mbio.01733-21
52. Cao M, Chen G, Wang L *et al.* Computational prediction and analysis for tyrosine post-translational modifications via elastic net. *J Chem Inf Model* 2018;**58**:1272–81. https://doi.org/10.1021/acs.jcim.7b00688
53. Trobridge G, Russell DW. Cell cycle requirements for transduction by foamy virus vectors compared to those of oncovirus and lentivirus vectors. *J Virol* 2004;**78**:2327–35. https://doi.org/10.1128/JVI.78.5.2327-2335.2004
54. Shogren-Knaak M, Ishii H, Sun J-M *et al.* Histone H4-K16 acetylation controls chromatin structure and protein interactions. *Science* 2006;**311**:844–7. https://doi.org/10.1126/science.1124000
55. Sinha D, Shogren-Knaak MA. Role of direct interactions between the histone H4 Tail and the H2A core in long range nucleosome contacts. *J Biol Chem* 2010;**285**:16572–81. https://doi.org/10.1074/jbc.M109.091298
56. Dodonova SO, Zhu F, Dienemann C *et al.* Nucleosome-bound SOX2 and SOX11 structures elucidate pioneer factor function. *Nature* 2020;**580**:669–72. https://doi.org/10.1038/s41586-020-2195-y
57. Hennig T, O'Hare P. Viruses and the nuclear envelope. *Curr Opin Cell Biol* 2015;**34**:113–21. https://doi.org/10.1016/j.ceb.2015.06.002
58. Dimitrova DS, Gilbert DM. The spatial position and replication timing of chromosomal domains are both established in early G1 phase. *Mol Cell* 1999;**4**:983–93. https://doi.org/10.1016/S1097-2765(00)80227-0
59. Sadoni N, Langer S, Fauth C *et al.* Nuclear organization of mammalian genomes. *J Cell Biol* 1999;**146**:1211–26. https://doi.org/10.1083/jcb.146.6.1211
60. Gholamalamdari O, Schaik Tv, Wang Y *et al.* Beyond A and B compartments: how major nuclear locales define nuclear genome organization and function. *eLife* 2024;**13**:RP99116. https://doi.org/10.1101/2024.04.23.590809
61. Jang S, Bedwell GJ, Singh SP *et al.* HIV-1 usurps mixed-charge domain-dependent CPSF6 phase separation for higher-order capsid binding, nuclear entry and viral DNA integration. *Nucleic Acids Res* 2024;**52**:11060–82. https://doi.org/10.1093/nar/gkae769

Received: March 3, 2025. **Revised:** May 5, 2025. **Editorial Decision:** May 6, 2025. **Accepted:** May 15, 2025